Available online at www.sciencedirect.com
ScienceDirect
Ceramics International 38 (2012) 741–746
CERAMICS INTERNATIONAL
www.elsevier.com/locate/ceramint

Structural and magnetic characterization of $Mn_xZn_{1-x}Fe_2O_4$ ($x = 0.2$; 0.35; 0.65; 0.8; 1.0) ferrites obtained by the citrate precursor method

R. Gimenes [a,*], M.R. Baldissera [a], M.R.A. da Silva [a], C.A. da Silveira [a], D.A.W. Soares [a], L.A. Perazolli [b], M.R. da Silva [a], M.A. Zaghete [b]

[a] Federal University of Itajubá – UNIFEI, Institute of Exact Sciences (ICE). Av. BPS, 1303, Postal Code 37500-903. Itajubá, MG, Brazil
[b] Microwave Sintering and Photocatalysis Laboratory, Instituto de Química de Araraquara, UNESP – Univ Estadual Paulista, R. Prof. Francisco Degni s/n, P.O. Box 355, 14800-900 Araraquara, SP, Brazil

Received 29 April 2011; received in revised form 28 July 2011; accepted 29 July 2011
Available online 5th August 2011

Abstract

In this work the microstructure and magnetic properties of Mn–Zn ferrites powders were investigated. $Mn_xZn1_{-x}Fe_2O_4$ powders where $x = 0.2$; 0.35; 0.5; 0.65; 0.8 and 1.0 were obtained by citrate precursor method. Citrate resin precursor was burned on air atmosphere at 400 °C for 3 h. Mn–Zn powders were calcined at 950 °C during 150 min under inert atmospheres: N_2 and rarefied atmosphere. Thermal analysis of precursor resin, phase evolution and microstructure of Mn–Zn ferrites powders were investigated by TG, DTA, XRD and SEM techniques. The powders calcined under rarefied atmosphere show spinel cubic structure and contamination of α-Fe_2O_3, while powders calcined under N_2 presents only the spinel cubic structure. Particle size was observed by SEM ranging from 80 to 150 nm. The magnetic properties were measured employing a vibrating sample magnetometer (VSM). It was observed that the saturation magnetization M_s increased with the increase of Mn content. The M_s of $Mn_{0.8}Zn_{0.2}Fe_2O_4$ calcined on rarefied atmosphere and $Mn_{0.8}Zn_{0.2}Fe_2O_4$ calcined on N_2 was 23.31 emu g^{-1} and 56.23 emu g^{-1}, respectively.

Keywords: C. Magnetic properties; Microstructure; Mn–Zn ferrite; Citrate precursor method

1. Introduction

Mn–Zn ferrites are one of the magnetic materials having wide applications, like soft magnetic powders, magnetic fluids, heat transfer systems [1,2], hard materials for transformer core, microwave absorption materials, high velocity magnetic record, makers for resonance magnetic imaging [3] and on magnetoelectric composites [4]. The Mn–Zn ferrites are preferred over other ferrites because of their high initial permeability, low losses, high saturation magnetization and relatively high Curie temperature [5]. These ceramics have spinel structure based on a face-centered cubic lattice of oxygen ions with functional units of $(Zn_xFe_{1-x})[Mn_{1-x}Fe_{1+x}]O_4$ [6].

It is well known that the final properties of Mn–Zn ferrites are strongly influenced by Zn–Mn ratio, microstructure of particles, and high sensitivity to the preparation methods [7–9]. While Mn–Zn ferrites obtained by dry methods, like mixture of oxides [10,11], show poor compositional control, larger particle size, and impurities, the wet chemical methods produce ultra fine and homogeneous powders, great control of particle size, and best magnetic performance. Several wet chemical methods have been used to synthesize ultra fine Mn–Zn ferrites powders, such as the citrate precursor method [12–14], autocombustion route [15,16], hydrothermal route [17–19] and sol–gel method [2,20].

To use MFe_2O_4 (where $M^{2+} = Mn^{2+}$, Zn^{2+}, Fe^{2+}, Co^{2+}, Ni^{2+}, etc.) for future magnetic microdevices that will integrate drug delivery systems a compromise between magnetic moment and absence of magnetic remanent memory is desirable, like on superparamagnetic particles [21]. Also promising is the use of magnetostrictive ferrite phase as trigger on magnetic-mechanically stimulated drug delivery systems. Nowadays highly magnetostrictive and resistive ferrite phases have become important materials of magnetoeletrostrictive composite (ME), which is used on a variety of smart materials [4,22].

* Corresponding author. Tel.: +55 35 36291438.
E-mail address: rossano@unifei.edu.br (R. Gimenes).

0272-8842/$36.00
doi:10.1016/j.ceramint.2011.07.066

Although it is known that the cobalt and nickel ferrites present good ME coefficients, the substitution of Mn on Co-ferrites increases the magnetostriction of materials [16]. Particle size is very important parameter to magnetic performance of Mn–Zn ferrites. Yáñes-Vilar [21] related superparamagnetic behavior to MFe_2O_4 ferrites nanoparticles with size around 10 nm. The deviation in normal cation distribution in which Mn^{2+} and Zn^{2+} occupied tetrahedral A site and Fe^{3+} occupied octahedral B site leads to tilts M_s, H_c and ME coefficients of Mn–Zn ferrites.

In this way, the citrate precursor method was used to fine control the cation stoichiometry and the particle size. Dielectric and magnetic properties of Mn–Zn ferrites obtained by citrate precursor method were investigated. We have also investigated the influence of atmosphere of calcination process on the crystalline structure of Mn–Zn ferrite.

2. Experimental

Ultrafine powders of Ferrites, composition $Mn_xZn_{1-x}Fe_2O_4$ where $x = 0.2$; 0.35; 0.65; 0.8; 1.0, were synthesized by citrate precursor method. For this, the following reactants of analytical grade were used: Manganese (II) acetate (Carlo Erba, Rodano, Italy), Ammonium Iron (III) Citrate (Vetec, Duque de Caxias, Brazil), Zinc oxide (Synth, Diadema, Brazil), Nitric Acid (Impex, Diadema, Brazil), citric acid (Synth, Diadema, Brazil), ethylene glycol (Synth, Diadema, Brazil). The solids reactants were weighed on stoichiometric proportion. Zinc oxide was dissolved on excess of concentrated nitric acid at room temperature and magnetic stirring. Aqueous solution of manganese (II) acetate was dripped on acid solution of zinc nitrate and was heated at 80 °C with constant stirring. After the total evaporation of acetic acid, under warming at 80 °C, aqueous solution of Ammonium Iron (III) Citrate and citric acid was slowly added on precursor solution with constant stirring at 50–60 °C to avoid precipitation. Citric acid was added on precursor solution to promote the chelating reaction between metallic cations and carboxylic groups. The pH of metals citrate complex solution was adjusted to 5–6. Ethylene glycol was added to citrate complex solution to promote the polysterification reaction to forming a viscous resin complex after heating at 60 °C during ∼2 h. During the synthesis of complexes, formation of precipitated cations was not observed. Viscous resin of citrate precursor with a uniformly brown coloured aspect was burned on furnace at 400 °C for 30 min and at 500 °C for 150 min, under injection of dried air. Samples of citrate precursor were characterized by thermogravimetric analysis TG/DTA (Netzsch model STA 409), up to 1000 °C at heating rate of 10 °C/min, air/O_2 atmosphere.

The burned citrate precursor was manually disaggregated on agate mortar and calcinated in a tubular furnace at 950 °C during 150 min under two different atmospheres: N_2 and atmosphere pressure under 0.01 bar (low vacuum – LV).

X-ray diffraction (XRD) of Mn–Zn ferrites powders was performed on a Rigaku diffractometer (Rint 2000) using Cu-K_α radiation (λ = 1.5406 A) employing a scanning rate 0.2° s^{-1} and 2θ ranging from 20° to 80°. The powders morphology was observed by scanning electron microscopy (SEM, Topcon, model SM300).

The magnetic properties of the Mn–Zn ferrites powders were measured with a room temperature vibrating sample magnetometer (VSM; LakeShore Model 7410) varying the magnetic field up to ±15 kG.

3. Results and discussion

3.1. Thermal decomposition of citrate precursor

Fig. 1 shows the TGA/DTA curves of $Mn_{0.2}Zn_{0.8}Fe_2O_4$, $Mn_{0.35}Zn_{0.65}Fe_2O_4$, $Mn_{0.5}Zn_{0.5}Fe_2O_4$, and $Mn_{0.65}Zn_{0.35}Fe_2O_4$ polymeric citrate precursor thermally treated from room temperature to 1000 °C. There are two weight loss processes occurring between temperatures at 100–380 °C (TG1) and 380–510 °C (TG2). The first step of weight loss is between 62% ($Mn_{0.65}Zn_{0.35}Fe_2O_4$) and 70% ($Mn_{0.2}Zn_{0.8}Fe_2O_4$) correspondent to volatilization of water and unreacted ethylene glycol, evidenced by the endothermic peak at 205 °C on the DTA curves, and decomposition of citric acid assigned to peaks at 310–320 °C. In the second step of weight loss, the weight loss is ∼23% ascribed to thermal decomposition of citrate precursors into oxides, evidenced by the presence of exothermic peaks at 430–510 °C.

Also, on DTA curves of $Mn_{0.2}Zn_{0.8}Fe_2O_4$ and $Mn_{0.35}Zn_{0.65}Fe_2O_4$ two exothermic peaks are seen at 430–510 °C while for $Mn_{0.5}Zn_{0.5}Fe_2O_4$ and $Mn_{0.65}Zn_{0.35}Fe_2O_4$ one broad peak is seen, suggesting that the nucleation of $ZnFe_2O_4$ and $MnFe_2O_4$ occur at different temperatures.

On TGA curves an increase in the weight after ∼500 °C is not seen, indicating that the oxidation process of $Mn^{2+} \rightarrow Mn^{4+}$ does not occur, unlike the results observed by Kambale et al. [15].

3.2. Structural analysis

Considering the TG/DTA analysis it can be inferred that the Mn–Zn ferrites could be obtained by calcination of citrate complex precursors at temperatures higher than 550 °C. The X-ray diffraction (XRD) technique was used to confirm the presence of crystalline phases and to study the influence of atmosphere on calcination process.

Fig. 2 shows XRD patterns of Mn–Zn ferrites calcined on rarefied atmosphere – low vacuum. The samples show all the characteristic reflections of cubic spinel structure of ferrite with the characteristic (3 1 1) reflection on $2\theta = 34.5°$. The XRD patterns were indexed using the JCPDS cards with goods agreements for $Mn_{0.2}Zn_{0.8}Fe_2O_4$ (card no. 74-2399), $Mn_{0.5}Zn_{0.5}Fe_2O_4$ (card no. 74-2401), $Mn_{0.8}Zn_{0.2}Fe_2O_4$ (card no. 74-2402). Also on XRD patterns it is possible to identify the presence of contaminant phase of α-Fe_2O_3 with good agreement with the JCPDS card no. 72-469.

The relative intensity of peaks of α-hematite increases with the increase of Mn content on ferrite structure, when the powders are calcined on oxidant atmosphere. The fact that the increase of α-hematite concentration is related with [Mn^{2+}] on precursor can be explained on account of site Mn^{2+} occupancy

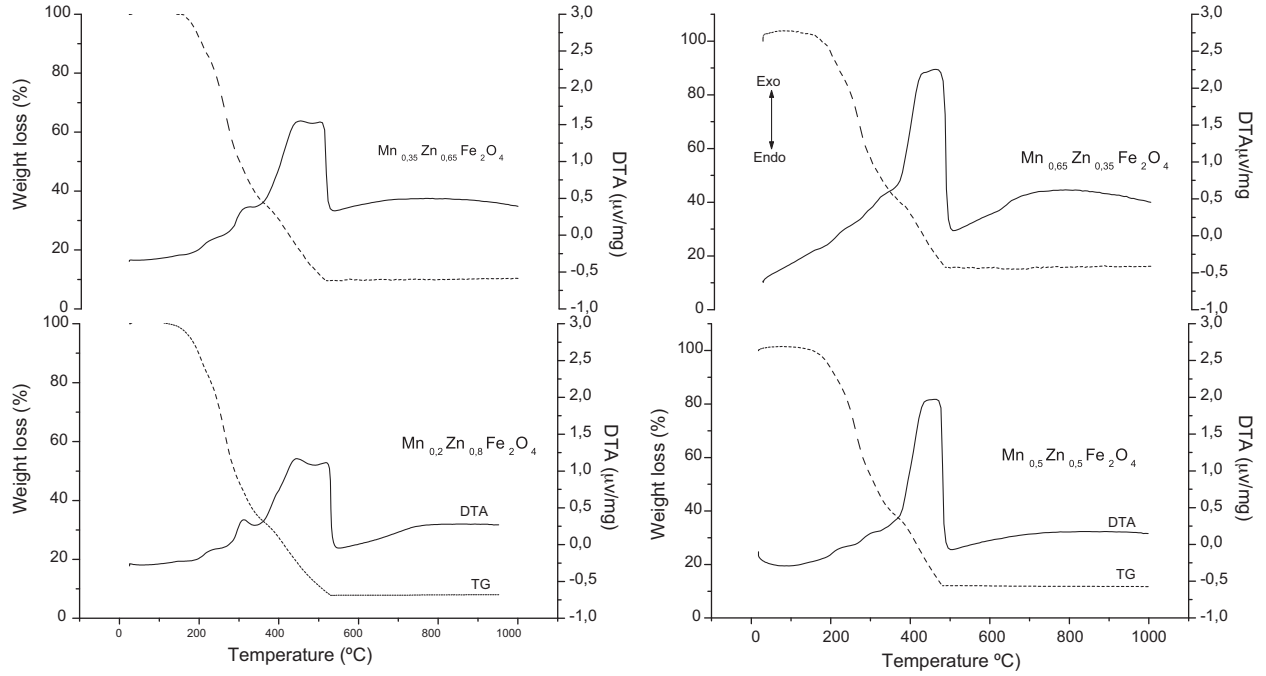

Fig. 1. TG–DTA curves of complex ferrites precursors.

tendency, which has strong preference for A (tetrahedral) sites, while Mn^{3+} has strong preference for B (octahedral) sites, and Zn^{2+} has strong specific affinity to A (tetrahedral) sites. The nucleation of $MnFe_2O_4$, nearly 20% of Mn, is located in the B sites as Mn^{3+}. For charge compensation an equivalent amount of iron ions will be as Fe^{2+} which is oxidized to Fe_2O_3 due to low capacity of air atmosphere to redeem the interstitial oxygen ions, according to reaction (1).

$$2FeO + (1/2)O_2 \leftrightarrow Fe_2O_3 + v''_{Fe} + O^x_O \quad (1)$$

Fig. 3 shows XRD patterns of Mn–Zn ferrites calcined at 950 °C on N_2 atmosphere. It is clear that all composition of Mn–Zn ferrites calcined on N_2 atmosphere have a highly pure cubic spinel structure, with all the characteristic reflections. The XRD patterns were indexed using the JCPDS card no. 74-2399, referent to cubic spinel structure and *Fd*-3*m* space group. No peaks were seen assigned to α-hematite or another iron rich phase.

The effect of inert atmosphere on crystallization of pure cubic spinel structure can be explained based on chemical instability of Fe^{3+} in the A sites, that on absence of oxygen, it will transfer electrons to Mn^{2+} in the B sites. This will stabilize both ions Fe^{2+} and Mn^{3+} in the A and B sites, respectively. In this way, two possible reaction mechanisms will result on

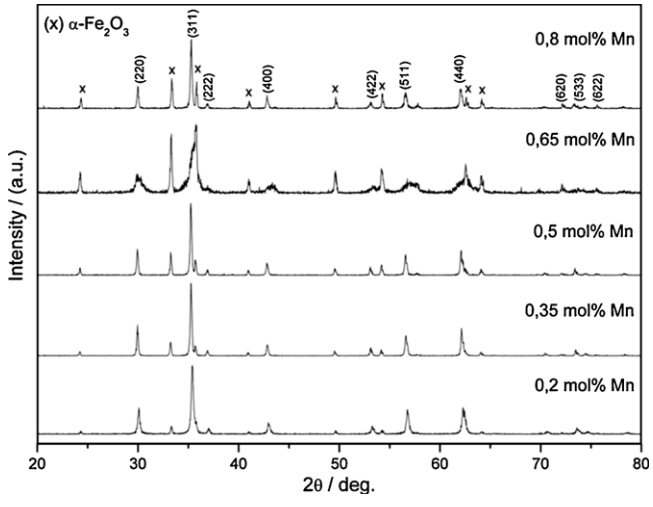

Fig. 2. X-ray diffraction patterns of Mn–Zn ferrites powders with different Mn contents, calcined at 950 °C in rarefied atmosphere, (*x*) α-Fe_2O_3.

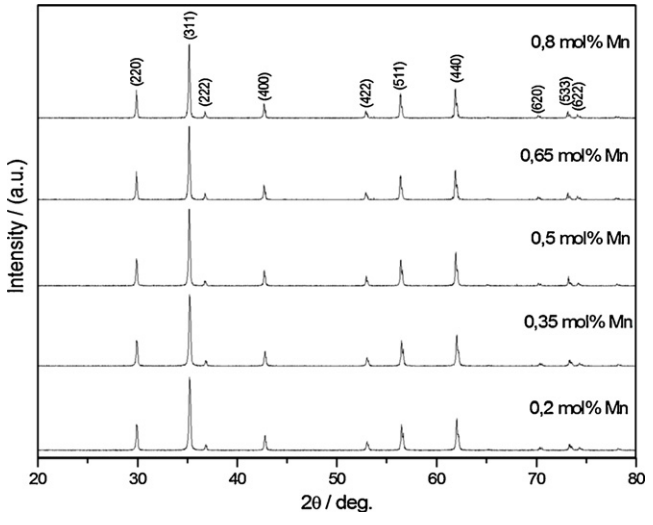

Fig. 3. XRD patterns of powders of Mn–Zn ferrites with different Mn contents, calcined at 950 °C in N_2 atmosphere.

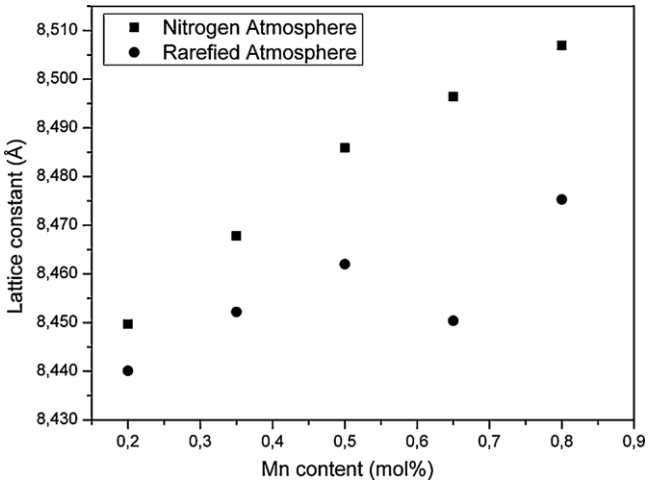

Fig. 4. Variation of lattice constant, a, in function of Mn content for Mn–Zn ferrites calcined at 950 °C.

Mn–Zn ferrites with different purity grades and cation distribution sites, represented by reactions (2) and (3).

$$[Zn^{2+}Mn^{2+}Fe^{3+}]O \xrightarrow{\downarrow PO_2} [Zn^{2+}Mn^{2+}_{1-x}Fe^{3+}_{x}]_A$$
$$[Mn^{2+}_{x}Fe^{3+}_{2-x}]_B O_4 \xrightarrow{\downarrow PO_2} [Zn^{2+}Mn^{2+}_{1-x}Fe^{3+}_{x-y}]_A$$
$$[Mn^{2+}_{x}Fe^{3+}_{2-x}]_B O_4 + yFe_2O_3 \quad (2)$$

$$[Zn^{2+}Mn^{2+}Fe^{3+}]O \xrightarrow{\downarrow N_2} [Zn^{2+}Mn^{2+}_{1-x}Fe^{3+}_{x}]_A$$
$$[Mn^{2+}_{x}Fe^{3+}_{2-x}]_B O_4 \xrightarrow{\downarrow N_2} [Zn^{2+}Mn^{2+}_{1-x}Fe^{2+}_{x}]_A$$
$$[Mn^{3+}_{x}Fe^{3+}_{2-x}]_B O_4 \quad (3)$$

where $[Zn^{2+}Mn^{2+}Fe^{3+}]O$ is an intermediary state of ferrite.

The mean crystallite size calculated from XRD line width of the (3 1 1) peak using the Scherrer's equation. From Table 1 it is observed that for powders calcined on N_2 atmosphere the crystallite size increases from 38 nm to 54 nm with increasing Mn^{2+} content. It is comprehensive considering that the nucleation and growth of crystallites are influenced by the probability of available site for cation occupancy. With three sites available for each unit cell (two octahedral, one tetrahedral), Mn^{2+} will have a higher probability of getting absorbed by a nucleus unlike the Zn^{2+} that only occupies the tetrahedral sites. In this way, the Mn^{2+} favors the nucleation process and growth of particles. Similar results were found by Rath et al. [6].

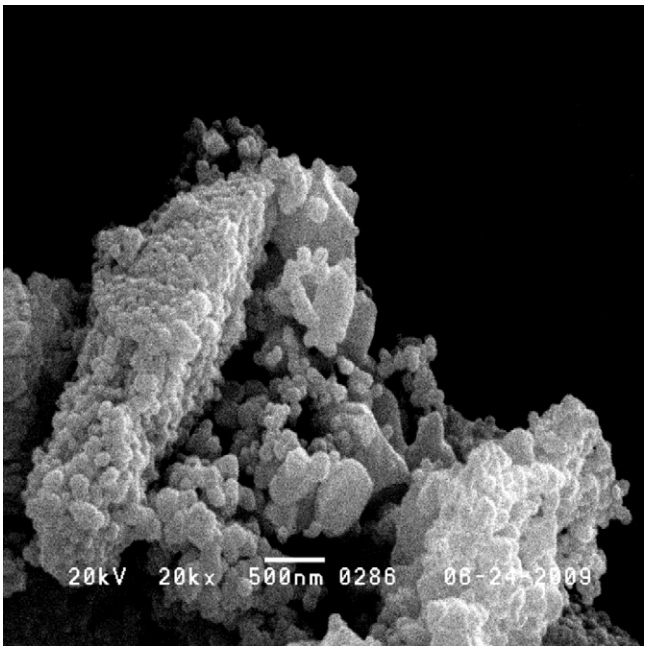

Fig. 5. SEM micrograph of $Mn_{0.8}Zn_{0.2}Fe_2O_4$ powder dispersed on ethanol using a sonicator (650 W power).

Fig. 4 shows the variation of lattice parameter *a* as function of Mn content obtained by refining of XRD data. On the powders calcined under N_2 atmosphere the lattice parameter increases linearly with increasing Mn content. The increase in lattice parameter can be attributed to replacement of smaller cation Zn^{2+} (0.74 Å) by larger Mn^{2+} (0.83 Å). Usually, in a solid solution within of miscibility limit of cubic phases a linear increment in the lattice parameter with concentration of cations is observed.

The morphology of $Mn_{0.8}Zn_{0.2}Fe_2O_4$ is shown in SEM micrograph of Fig. 5. For all compositions the Mn–Zn ferrites show similar morphology of particles. In Fig. 5 is seen spherical morphology of particles with very strong agglomeration due to magnetic characteristic of particles. These agglomerates were not broken by ultrasonic horn with 650 W power applied for a few minutes. The average particle size ranged from 80 to 150 nm.

3.3. Magnetic properties

Figs. 6 and 7 show the *M–H* loop for Mn–Zn ferrites calcined on low vacuum and N_2 atmosphere, respectively. The variation of saturation magnetization (M_s) with Mn content is shown in

Table 1
Crystallite size calculated from X-ray peak broadening of the (3 1 1) peak using the Scherrer's equation.

Sample calcinated on low vaccum	Crystallite size (nm)	Sample calcinated on N_2 atmosphere	Crystallite size (nm)
$Mn_{0.2}Zn_{0.8}Fe_2O_4$	35	$Mn_{0.2}Zn_{0.8}Fe_2O_4$	38
$Mn_{0.35}Zn_{0.65}Fe_2O_4$	48	$Mn_{0.35}Zn_{0.65}Fe_2O_4$	41
$Mn_{0.5}Zn_{0.5}Fe_2O_4$	48	$Mn_{0.5}Zn_{0.5}Fe_2O_4$	48
$Mn_{0.65}Zn_{0.35}Fe_2O_4$	15	$Mn_{0.65}Zn_{0.35}Fe_2O_4$	51
$Mn_{0.8}Zn_{0.2}Fe_2O_4$	44	$Mn_{0.8}Zn_{0.2}Fe_2O_4$	54

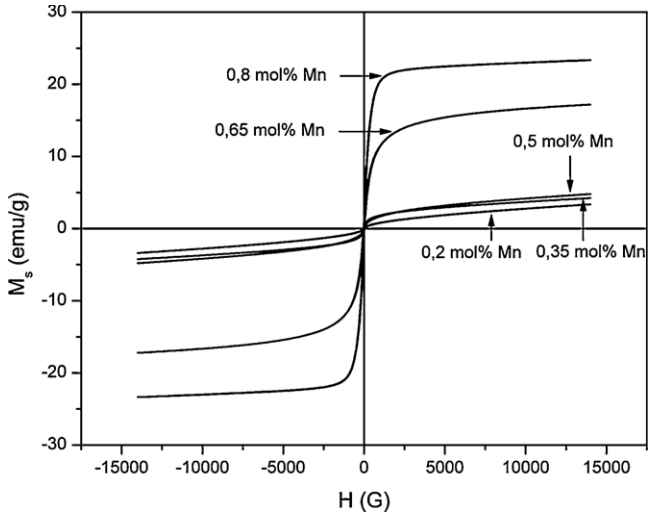

Fig. 6. Hysteresis loops of the Mn–Zn ferrites calcined at 950 °C, in the rarefied atmosphere.

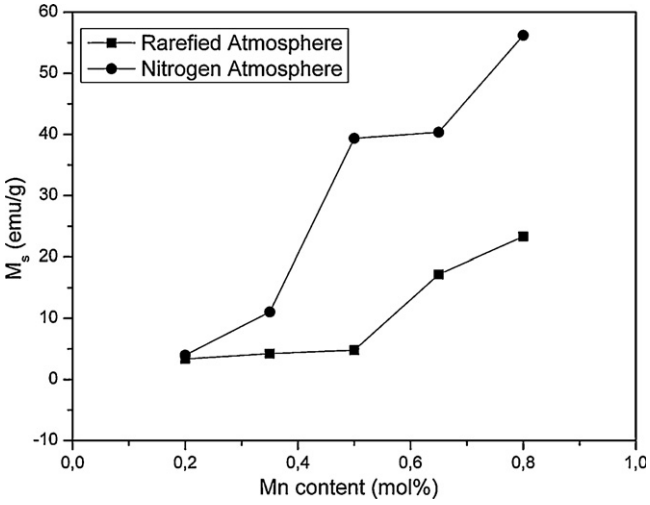

Fig. 8. Variation of the saturation magnetization M_s with Mn content at room temperature.

Fig. 8. It is seen that both M_s and M_r (Table 2, Fig. 8) increase from 0.064 and 3.35 emu g^{-1}, respectively for $Mn_{0.2}Zn_{0.8}Fe_2O_4$ to 1.09 and 23.31 emu g^{-1} for $Mn_{0.8}Zn_{0.2}Fe_2O_4$. The increase in the magnetization of Mn–Zn ferrites for composition rich on Mn^{2+} is expected since Mn^{2+} has magnetic moment of 5 μ_B while Zn^{2+} is diamagnetic. When the Mn^{2+} replaces the Zn^{2+} on the A sites there will be magnetic interaction Mn–Mn. This behavior is illustrated considering that the bulk Mn–ferrite exhibits a M_s between 55 and 80 emu g^{-1} while ZnF_2O_4 is paramagnetic until 9.5 K [17]. Analyzing the *M–H* hysteresis loops, shown in Figs. 6 and 7, it was obtained a soft ferrites powders by citrate precursor method.

The M_s and M_r values for Mn–Zn ferrites calcined on N_2 atmosphere are larger than obtained for ferrites calcined on low vacuum, indicating that the presence of α-Fe_2O_3 decreases the magnetization of Mn–Zn ferrites, since the α-Fe_2O_3 acts as antiferromagnetic material.

Table 2
Saturation magnetization, remanent magnetization and coercitivity magnetic field of Mn–Zn ferrites powders.

Sample	M_s (emu g^{-1})	M_r (emu g^{-1})	H_c (kG)
Panel A – calcined on low vaccum			
$Mn_{0.2}Zn_{0.8}Fe_2O_4$	3.35	0.064	0.034
$Mn_{0.35}Zn_{0.65}Fe_2O_4$	4.21	0.096	0.015
$Mn_{0.5}Zn_{0.5}Fe_2O_4$	4.78	0.15	0.028
$Mn_{0.65}Zn_{0.35}Fe_2O_4$	17.17	0.97	0.0028
$Mn_{0.8}Zn_{0.2}Fe_2O_4$	23.31	1.09	0.018
Panel B – calcined on N_2 atmosphere			
$Mn_{0.2}Zn_{0.8}Fe_2O_4$	3.98	0.013	0.0048
$Mn_{0.35}Zn_{0.65}Fe_2O_4$	11.04	0.080	0.0031
$Mn_{0.5}Zn_{0.5}Fe_2O_4$	39.37	1.74	0.019
$Mn_{0.65}Zn_{0.35}Fe_2O_4$	40.37	3.56	0.043
$Mn_{0.8}Zn_{0.2}Fe_2O_4$	56.23	7.08	0.0072

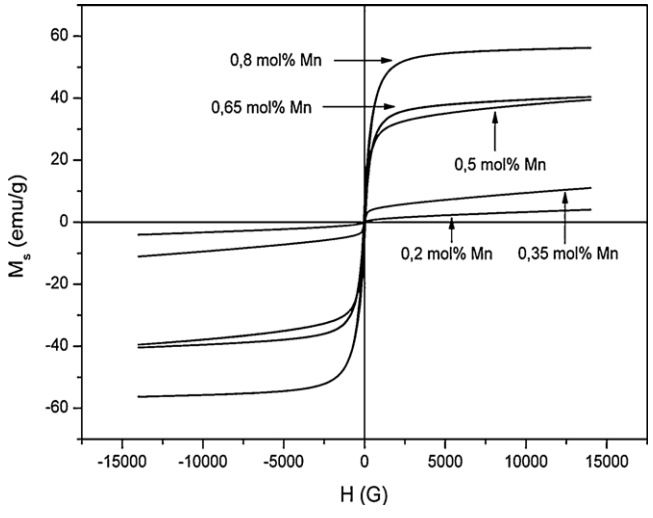

Fig. 7. Hysteresis loops of the Mn–Zn ferrites calcined at 950 °C, in the N_2 atmosphere.

Considering that at larger Mn concentration ($x = 0.65$ and 0.8) Mn^{2+} (5 μ_B) is replaced for Fe^{2+} (4 μ_B) on A sites and an equivalent amount of Fe^{3+} is substituted by Mn^{3+} (4 μ_B) on the B sites. Then the magnetization of ferrite was expected to decrease, since in the booth A and B sites is replaced a 5 μ_B by 4 μ_B cations, but analyzing the data displayed in Table 2, this does not occur. A possible explanation is based on increasing contribution of the magnetocrystalline anisotropy when Zn is substituted for Mn.

4. Conclusions

Fine and crystalline soft Mn–Zn ferrites powders can be easily obtained from the citrate precursor method. Mn–Zn ferrites calcined at 950 °C under N_2 atmosphere were found to have pure cubic spinel structure with space group *Fd*-3*m*. Ferrites calcined on air atmosphere at low pressure presents α-Fe_2O_3 contamination. Magnetic properties are influenced by the different contribution of magnetic moment of substituted

cations on A and B sites, as well as magnetocrystalline anisotropy. The best magnetization was found for ferrite $Mn_{0.8}Zn_{0.2}Fe_2O_4$ with M_s, M_r and H_c equal 56.23 emu g^{-1}, 7.08 emu g^{-1} and 0.0072 kG, respectively.

Acknowledgements

Authors would like to thank CAPES, CNPq, FAPEMIG and FAPESP for financial support.

References

[1] B. Jeyadevan, C.N. Chinnasamy, K. Shinoda, K. Tohji, Mn–Zn ferrite with higher magnetization for temperature sensitive magnetic fluid, J. Appl. Phys. 93 (2003) 8450–8452.
[2] J. Azadmanjiri, Preparation of Mn–Zn ferrite nanoparticles from chemical sol–gel combustion method and the magnetic properties after sintering, J. Non-Cryst. Sol. 353 (2007) 4170–4173.
[3] S. Gubbala, H. Nathani, K. Koizol, R.D.K. Misra, Magnetic properties of nanocrystalline Ni–Zn, Zn–Mn, and Ni–Mn ferrites synthesized by reverse micelle technique, Physica B 348 (2004) 317–328.
[4] N. Cai, J. Zhai, C.W. Nan, Y. Lin, Z. Shi, Dielectric, ferroelectric, magnetic, and magnetoelectric properties of multiferroic laminated composites, Phys. Rev. B 68 (2003) 224103.
[5] C.F. Zhang, X.C. Zhong, Y.H. Yu, Z.W. Liu, D.C. Zeng, Effects of cobalt doping on the microstructure and magnetic properties of Mn–Zn ferrites prepared by the co-precipitation method, Physica B 404 (2009) 2327–2331.
[6] C. Rath, S. Anand, R.P. Das, K.K. Sahu, S.D. Kulkarni, S.K. Date, N.C. Mishra, Dependence on cation distribution of particle size, lattice parameter, and magnetic properties in nanosize Mn–Zn ferrite, J. Appl. Phys. 91 (2002) 2211–2215.
[7] A. Verma, T.C. Goel, R.G. Mendiratta, M.I. Alam, Dielectric properties of NiZn ferrites prepared by the citrate precursor method, Mater. Sci. Eng. B 60 (1999) 156–162.
[8] H.N. Choi, K.S. Baek, S.W. Hyun, I. Shim, C.S. Kim, A study of co substituted Mn–Ferrite, $Mn_{1-x}Co_xFe_2O_4$ ($x = 0.0,0.5,1.0$), IEEE Trans. Magnet. 45 (2009) 2554–2556.
[9] X.M. Liu, S.Y. Fu, H.M. Xiao, L.P. Zhu, Preparation and characterization of complex ferrite nanoparticles by a polymer-pyrolysis route, J. Nanoparticle Res. 9 (2007) 1041–1046.
[10] J. Moulin, Y. Champion, J.M. Greneche, F. Mazaleyrat, Magnetic properties of MnZn ferrite with ultra-fine grain structure, J. Magn. Magn. Mater. 254 (2003) 538–540.
[11] A. Angermanna, J. Topfera, K.L. Silva, K.D. Becker, Nanocrystalline Mn–Zn ferrites from mixed oxalates: synthesis, stability and magnetic properties, J. Alloys Compd. 508 (2010) 433–439.
[12] A. Thakur, M. Singh, Preparation and characterization of nanosize $Mn_{0.4}Zn_{0.6}Fe_2O_4$ ferrite by citrate precursor method, Ceram. Int. 29 (2003) 505–511.
[13] A. Verma, R. Chatterjee, Effect of zinc concentration on the structural, electrical and magnetic properties of mixed Mn–Zn and Ni–Zn ferrites synthesized by the citrate precursor technique, J. Magn. Magn. Mater. 306 (2006) 313–320.
[14] B.S. Randhawa, H.S. Dosanjh, M. Kaur, Preparation of spinel ferrites from citrate precursor route—a comparative study, Ceram. Int. 35 (2009) 1045–1049.
[15] R.C. Kambale, P.A. Shaikh, C.H. Bhosale, K.Y. Rajpure, Y.D. Kolekar, The effect of Mn substitution on the magnetic and dielectric properties of cobalt ferrite synthesized by an autocombustion route, Smart Mater. Struct. 18 (2009) 115028.
[16] R.C. Kambale, P.A. Shaikh, N.S. Harale, V.A. Bilur, Y.D. Kolekar, C.H. Bhosale, K.Y. Rajpure, Structural and magnetic properties of $Co_{1-x}Mn_xFe_2O_4$ ($0 \leq x \leq 0.4$) spinel ferrites synthesized by combustion route, J. Alloys Compd. 490 (2010) 568–571.
[17] C. Upadhyay, H.C. Vermaa, C. Ratha, K.K. Sahub, S. Anande, R.P. Dasc, N.C. Mishrad, Mössbauer studies of nanosize $Mn_{1-x}Zn_x Fe_2O_4$, J. Alloys Compd. 326 (2001) 94–97.
[18] C.S. Hwang, N.C. Wang, Preparation and characteristics of ferrite catalysts for reduction of CO_2, Mater. Chem. Phys. 88 (2004) 258–263.
[19] L. Nalbandian, A. Delimitis, V.T. Zaspalis, E.A. Deliyanni, D.N. Bakoyannakis, E.N. Peleka, Hydrothermally prepared nanocrystalline Mn–Zn ferrites: synthesis and characterization, Micropor. Mesopor. Mater. 114 (2008) 465–473.
[20] P.P. Hankare, R.P. Patil, U.B. Sankpal, S.D. Jadhav, K.M. Garadkar, S.N. Achary, Synthesis and morphological study of chromium substituted Zn–Mn ferrites nanostructures via sol–gel method, J. Alloys Compd. 509 (2011) 276–280.
[21] S. Yáñes-Vilar, M. Sanchez-Andújar, C. Gómes-Aguirre, J. Mira, M.A. Señarís-Rodríguez, S. Castro-García, A simple solvothermal synthesis of MFe_2O_4 (M = Mn, Co and Ni) nanoparticles, J. Solid State Chem. 182 (2009) 2685–2690.
[22] C.W. Nan, Y. Lin, J.H. Huang, Magnetoelectricity of multiferroic composites, Ferroelectrics 280 (2002) 153–163.